CARMA Memorandum Series #38

Image Fidelity as a Function of Source Size and Calibration Errors.

M. C. H. Wright

Radio Astronomy laboratory, University of California, Berkeley, CA, 94720

January 3, 2007

ABSTRACT

In this memo we simulate observations with the CARMA telescope and calculate the image fidelity as a function of source size, pointing and calibration errors. We explore the effects of calibration errors on incorporating single dish data with interferometer observations. These results can be used in planning observations with the CARMA telescope.

We simulated observations using an image of Cas A scaled to different diameters as a source model. Simulated uv data sampled by the heterogeneous array of 10.4, 6.1, and 3.5 m antennas were used to make images at 230 GHz.

The different antenna diameters and primary beam sizes allow sources up to $\sim$ 32$''$ diameter to be observed with a single pointing center using the 15-antenna D-configuration at 230 GHz. Because of the different primary beam sizes, the data must be treated as a mosaic observation. The image fidelity decreases as the source size increases. Sources up to $\sim$ 64$''$ diameter can be observed with a 7-pointing hexagonal mosaic using the 15-antenna D-configuration at 230 GHz.

The image fidelity decreases when calibration errors are introduced. If calibration errors are small, (1%), then a joint deconvolution gives the best image fidelity. The image fidelity is very dependent on high quality single dish data. For amplitude fluctuations greater than $\sim$ 5% the best image fidelity is obtained using MOSMEM with a default single dish image rather than the joint deconvolution which gives more weight to the single dish data

The fidelity is greatly improved by mosaicing with the 23-antenna DZ configuration. The short interferometer spacings obtained with the 3.5m antennas provide much more robust information on the large scale structure and cross calibrate the single dish and interferometer observations.

Change Record

Revision	Date	Author	Sections/Pages Affected
			Remarks
1.1	2006-Dec-16	MCHW	1-6
	Draft memo		
1.1	2006-Dec-22	MCHW	1-15
	Draft memo		
1.1	2006-Dec-29	MCHW	1-17
	Better abstract, intro.		
1.1	2006-Dec-30	MCHW	1-17
	add primary beam plot and discussion.		

1. Introduction

The CARMA telescope is a heterogeneous array of 10.4, 6.1 and 3.5 m antennas, with antenna configurations providing spacings from $\sim$ 4 m to 2 km. This heterogeneous array is well suited to imaging a wide range of spatial scales.

A 10.4 m antenna at a wavelength of λ 1.3 mm has a field of view of $\sim 30''$; sources larger than this require a mosaic of interferometer and single dish observations at multiple pointing centers. The case for a homogeneous array has been well studied (e.g. Cornwell, Holdaway & Uson, 1993; Holdaway, 1998). The image fidelity for mosaic observations is limited by pointing and primary beam errors (Cornwell, Holdaway & Uson, 1993).

For the CARMA telescope, the different antenna diameters provide good cross calibration of the multiple primary beam patterns. The central hole in the uv sampling is smaller which means that there is less information which must be obtained from single dish observations. If we use the 10.4 m antennas to obtain the single dish observations, there is a large region of overlap in spatial frequencies which can be used to cross calibrate the single dish and interferometer observations. The heterogeneous interferometer observations also provide an excellent cross calibration of the 3.5, 6.1 and 10.4 m antennas.

However, there are calibration errors from system temperature and sky opacity variations, antenna gain versus elevation, pointing and primary beam errors etc., and the effect of these errors on image fidelity is a function of the source size, and the way in which single dish data is incorporated into the images.

In this memo, we investigate the effect of image size and calibration errors on the image fidelity for small mosaics. We explore the effects of these amplitude errors for four different algorithms for incorporating single dish data with interferometer observations. These results can be used in planning observations of extended sources.

2. Imaging with a Heterogeneous Array

Because of the different primary beam sizes, imaging with a heterogeneous array must be treated as a mosaic observation even when only a single concentric pointing center is used for all antennas. For a point source at the pointing center, e.g. a quasar calibration observation, the array response is well described by the forward gain for each baseline. For the CARMA telescope, the forward gain, in Jy/K units, is given in Table 1 for each antenna pair assuming an aperture efficiency 75% for all antennas. The equivalent diameter and forward gain were calculated from the geometric mean for each antenna pair.

However for a source which is not at the pointing center, the array response depends on the primary beam pattern for each antenna pair. The FWHM at 230 GHz is given in Table 1 assuming

a Gaussian primary beam pattern for each antenna. Clearly, a point source at the FWHM for a 6.1 m antenna will have very different amplitudes for 10.4 x 10.4, 10.4 x 6.1, and 6.1 x 6.1 m. antenna pairs, and will not be well represented as a point source (which has constant amplitude) unless account is taken for the different primary beam patterns for each antenna pair. The array response is easily modeled by the MIRIAD task *uvgen* by using the appropriate primary beam model for each antenna pair. If proper account is not taken of the different primary beam response for each antenna pair, the systematic amplitude difference on different interferometer baselines rapidly degrades the image fidelity with increasing source distance from the pointing center. E.g. for a source 6″ from the pointing center the primary beam response (and the point source amplitude) is 0.88, 0.92 and 0.96 for 10.4 x 10.4, 10.4 x 6.1, and 6.1 x 6.1 m. antenna pairs respectively, and the image fidelity (Peak/RMS noise) is decreased by a factor of 3 if the amplitudes are not corrected for the primary beam response. At 20″ from the pointing center the image is badly distorted by the amplitude differences between different antenna pairs. Observations of extended sources with a heterogeneous array must be treated as mosaic observations even when only a single concentric pointing center is used for all antennas.

A corrolary from the above discussion is that the image fidelity is degraded by pointing and primary beam errors. A 6″ pointing error results in 12%, 8% and 4% amplitude errors on 10.4 x 10.4, 10.4 x 6.1, and 6.1 x 6.1 m. baselines for a source at the nominal pointing center with a corresponding loss in image fidelity. For Gaussian primary beam patterns, the amplitude error is proportional to distance from the pointing center, but in a mosaic image, the data, and the errors, are weighted by the primary beam response. The primary beam response for a heterogeneous array is discussed in more detail in CARMA memo 5. The image fidelity for mosaic observations with a heterogeneous array is limited by pointing and primary beam errors

3. Primary Beam Response for Mosaic Images

For a single pointing observation, the image is usually not corrected for the primary beam pattern, as this correction can cause excessive noise amplification at the edge of the primary beam. In a mosaic image the effective primary beam response and the noise are a function of position. To avoid noise amplification at the edge of mosaiced regions, MIRIAD does not normally totally correct for the primary beam beyond a certain point. (see Sault, Staveley-Smith and Brouw, 1996, and the MIRIAD Users Guide for a more extensive discussion). The MIRIAD task *mossen* determines the effective primary beam response and the sensitivity for a mosaiced image.

Figure 1 shows the primary beam response for a single pointing mosaic with six 10.4 and nine 6.1m antennas (hex1-15), a 7-pointing hexagonal mosaic with 15 antennas (hex7-15), and the 23-antenna CARMA array (hex1-23). The primary beam pattern for 10.4, 6.1 and 3.5m antennas are also plotted for comparison.

4. Mosaicing Simulations

We made mosaicing simulations for compact configurations of the CARMA 15- and 23-antenna array using a model image of Cas A scaled to different diameters. *uv* data were created for each pointing center and primary beam pattern. Thermal noise, using a double sideband receiver temperature 80 K and a zenith opacity 0.26 at 230 GHz, was added to the *uv* data. We used a bandwidth 4 GHz and the antenna gains listed in Table 1 assuming an aperture efficiency 75% . *uv* data were sampled from -2 to +2 hours which gives good azimuthal *uv* coverage and minimizes antenna shadowing (see CARMA memo 5). Amplitude calibration errors were simulated by multiplying the *uv* data by random gain variations for each antenna on a 30 min time scale, commensurate with the typical calibration interval, and errors from antenna pointing and primary beam variations.

We made simulations for single pointing and 7-pointing hexagonal patterns with 15″ spacing. The thermal noise in the image for each sub-array and pointing center is listed in Table 1.

The *uv* data were Fourier transformed to make images and deconvolved using Maximum Entropy (MEM) algorithms. The image fidelity was calculated from the difference between the MEM image and the original image model convolved to the same resolution by a Gaussian restoring beam.

The simulations were made using standard MIRIAD programs using a csh script which generates *uv* data with added thermal noise and multiplicative amplitude errors for each antenna. This is a development of the same script used for ALMA, ATA, and previous CARMA simulations as described in earlier memos.

We made simulations for small source sizes which would fit within a single pointing or a hexagonal 7-pointing mosaic pattern. We explored the limitations of source and image size for obtaining the best image fidelity for each simulation. In all cases we used concentric pointing of all (six 10.4m, nine 6.1m, and for the 23-antenna array, eight 3.5m antennas). Amplitude gain errors were scaled to the antenna diameter to simulate the same RMS pointing errors on 10.4, 6.1, and 3.5m antennas, and natural weighting of the data in the imaging process.

Table 1: CARMA Primary Beam FWHM, Gain and Thermal Noise at 230 GHz

Antennas	Equivalent diameter	FWHM	Gain	Thermal noise
m x m	m	arcsec	Jy/K	mJy
10.4 x 10.4	10.4	28	43	0.76
10.4 x 6.1	8.0	36	73	0.69
6.1 x 6.1	6.1	47	126	1.4
10.4 x 3.5	6.0	48	128	1.7
6.1 x 3.5	4.6	63	220	2.4
3.5 x 3.5	3.5	83	383	9.5

5.   Results

Three different MEM deconvolutions were used: i) Using the interferometer data only with a total flux constraint. Single dish data were not included. ii) Using the single dish data as a default image. In this case, spatial frequencies obtained from the interferometer data replace those from the single dish data. iii) Joint deconvolution of the interferometer and single dish data. In this case, the extent to which the single dish data can be deconvolved is limited by our characterization of the primary beam and pointing errors in the single dish data. These three deconvolutions are compared in adjacent entries in the tables for each mosaic pattern, source size, and amplitude noise. The residual imaging errors are characterized by the total recovered flux, peak flux density and the RMS residuals. The image fidelity is listed in the last column as the ratio of the peak flux density to the on-source RMS in the residual image. The RMS was evaluated in a $50''$ bounding box.

5.1.   Mosaicing with CARMA-15 using single pointing mosaic

The image size was chosen so that the deconvolved image fits within the central quarter of the image plane. For a source diameter less than $\sim 40''$ an image size=129 is adequate. The results for a single pointing mosaic with 1% gain noise are shown in table 2. The image fidelity decreases as the source size increases from $16''$ to $40''$. For 1% amplitude fluctuations, the joint deconvolution of interferometer and single dish data gives better image fidelity than MOSMEM with a default single dish image, and this in turn is better than MOSMEM Interferometer only with a total flux constraint. This reflects the high quality of the single dish data. 1% amplitude errors are probably unrealistic. For a source diameter greater than $32''$ we used an image size=257. The results for a source diameter less $32''$ are almost identical to those obtained with an image size=129. An image size 257 permits single pointing mosaics for a source diameter up to $\sim 64''$.

In table 3, we show the effect of random amplitude fluctuations on a 0.5 hour time scale. For amplitude fluctuations greater than $\sim 5\%$, the best image fidelity is obtained using MOSMEM with a default single dish image rather than the joint deconvolution which gives more weight to, and gets larger errors from, the single dish data. Pointing errors are simulated as antenna dependent gain errors proportional to antenna size. With 20% amplitude errors there is little advantage of adding single dish data either as a default single dish image or in a joint deconvolution of interferometer and single dish data.

5.2.   Mosaicing with CARMA-15 using a 7-pointing mosaic

For the hexagonal 7-pointing mosaic we see the same pattern as the single pointing mosaic; for amplitude fluctuations greater than $\sim 5\%$ the best image fidelity is obtained using MOSMEM with a default single dish image rather than the joint deconvolution which gives more weight to

the single dish data (Table 4). The image fidelity for a $64''$ diameter source is improved by the 7-pointing mosaic if a default single dish MEM algorithm is used to deconvolve the mosaic image. Using only interferometer data or a joint deconvolution with single dish data, the image fidelity for the 7-pointing mosaic is lower than with a single pointing mosaic. The peak flux is better recovered by the 7-pointing mosaic, but the total flux is poorly estimated, and this results in a lower image fidelity measure. If the amplitude errors are small (1%), then a joint deconvolution (line 6 in table 4), gives the best image fidelity. For a $64''$ diameter source the image fidelity is very dependent on the quality of the single dish data.

5.3. Mosaicing with CARMA 23-antenna DZ configuration using a single pointing mosaic

The image fidelity is greatly improved by mosaicing with the CARMA 23-antenna DZ configuration (see CARMA memo 25). In a single concentric pointing the short interferometer spacings obtained with the 3.5m antennas provide much more robust information on the large scale structure as evidenced by the high image fidelity and good agreement between the peak and total recovered flux in the deconvolved and model images (table 5). Figure 6 shows the joint deconvolution for the DZ configuration. The DZ configuration provides a well sampled uv coverage and a very clean deconvolution with little of the flux density scattered out of the model image by poor uv sampling.

6. Discussion

With 1% amplitude errors, the best image fidelity was obtained using the joint deconvolution of the interferometer and single dish data. The extent to which the single dish data can be deconvolved is limited by calibration, primary beam and pointing errors in the single dish data, as well as thermal noise and systematic residual errors such as ground pickup or atmospheric fluctuations.

For the single dish data, we used the 10.4 m antennas, and set the noise at the same level as the RMS gain fluctuations in the interferometer observations, since we want the noise estimate for the single dish data to include primary beam and pointing errors. More than one 10.4 m antenna can, and should, be used to reduce random and systematic noise from pointing, primary beam and atmospheric fluctuations, but the data are treated here as one antenna with the same gain variations.

Using the single dish data as a default image, provides both a total flux estimate and low spatial frequencies unsampled by the interferometric mosaic. This gives higher image fidelity than just using the interferometer data with a total flux estimate. Giving higher weight to the single dish data, as in the joint deconvolution, improves the image fidelity, but a 1% error may be unrealistic.

For amplitude fluctuations greater than $\sim 5\%$ the best image fidelity is obtained using MOSMEM

with a default single dish image in both the single pointing and 7-pointing mosaic with the CARMA D-configuration.

For a $64''$ diameter source the image fidelity is very dependent on the quality of the single dish data. This can be undestood as resulting from the poor sampling of low spatial frequencies which overlap with the single dish data in the CARMA D-configuration. The 7-pointing mosaic improves this sampling, but it is still poor. Better image fidelity can be obtained by combining with CARMA E-configuration which provides shorter antenna spacings. The default image, provides a total flux estimate and low spatial frequencies unsampled by the interferometric mosaic. For combining images with very different resolutions, better results can be obtained using the MIRIAD task *immerge* to linearly merge together the single dish and interferometer images. *immerge* assumes that the low resolution single dish image better represents the short spacing data, whereas the high resolution interferometer image best represents the fine structure. The low resolution single-dish observation, and the high resolution mosaiced interferometric observation complement each other. (see Table)

The 23-antenna DZ configuration gives much better image fidelity, and is more robust to amplitude fluctuations, than the 15-antenna D configuration. Comparison of the model and mosaic images of Cas A scaled to $64''$ diameter observed with the CARMA 15-antenna D configuration using a hex7 pointing pattern (Figure 7) and observed with the CARMA 23-antenna DZ configuration using a single pointing center (Figure 8) show the much better imaging of the large scale structure obtained with the 23-antenna DZ configuration. The improvement in image fidelity from 15 to 108 makes a huge difference for quantitative analysis when comparing images to determine line ratios or spectral index variations across a source strucure. For example, the model of Cas A used in these simulations is a VLA image at 11.2 GHz. The simulations show that when imaged with the 15-antenna D configuration at 230 GHz, imaging errors would be confused with spectral index variations at the $\sim 6\%$ level. Using the 23-antenna DZ configuration we could map spectral index variations across the source at the $\sim 1\%$ level.

7. Conclusion

The heterogeneous CARMA telescope provides some interesting challenges and advantages compared with homogeneous arrays.

The different antenna diameters and primary beam sizes allow sources up to $\sim 32''$ diameter to be observed with a single pointing center using the 15-antenna D-configuration at 230 GHz. Because of the different primary beam sizes, the data must be treated as a mosaic observation. The image fidelity decreases as the source size increases. Sources up to $\sim 64''$ diameter can be observed with a 7-pointing hexagonal mosaic using the 15-antenna D-configuration at 230 GHz.

The image fidelity decreases when amplitude calibration errors are introduced. If amplitude errors are small (1%), then a joint deconvolution gives the best image fidelity. The image fidelity is very

dependent on high quality single dish data. For amplitude fluctuations greater than $\sim 5\%$ the best image fidelity is obtained using MOSMEM with a default single dish image rather than the joint deconvolution which gives more weight to the single dish data

The fidelity is greatly improved by mosaicing with the 23-antenna DZ configuration. In a single concentric pointing, the short interferometer spacings obtained with the 3.5m antennas provide much more robust information on the large scale structure and cross calibrate the single dish and interferometer observations.

8.   References

BIMA memo 45, *BIMA Array response to extended structure*, M.C.H. Wright, 1999, http://bima.astro.umd.edu/

BIMA memo 73, *Image Fidelity*, M.C.H. Wright, 1999, http://bima.astro.umd.edu/memo/memo.html

Sault, R.J., Staveley-Smith, L & Brouw, W.N., 1996, *An approach to interferometric mosaicing*, A&A Supp., 120, 375

Bob Sault & Neil Killeen, 1999, *Miriad Users Guide*, http://www.atnf.csiro.au/computing/software/miriad

Holdaway. M.A., 1999, *Mosaicing with Interferometer Arrays*, ASP Conference series 180, 401.

Cornwell, T.J., Holdaway, M.A. & Uson, J.M., 1993, *Radio-interferometric imaging of very large objects: implications for array design*, A&A 271, 697.

CARMA memo 5, *Compact Configuration Evaluation for CARMA*, Melvyn Wright, Sep 2002.

CARMA memo 25, *SZA location at CARMA site*, Melvyn Wright, June 2004.

Holdaway, M. A., 1998, *Mosaicing with Interferometer Arrays*, in Synthesis Imaging in Radio Astronomy II, ASP Conference Series, G. B. Taylor, C. L. Carilli and R. A. Perley (eds)

Table 2: Mosaicing Simulations for Cas A at 230 GHz. Using single pointing hex1-15.csh mosaic with 1% Gain Noise For each source size we lists three methods: i) MEM deconvolution with total flux constraint, 732.069 Jy, ii) using single dish as a default image, iii) joint deconvolution of interferometer and single dish data.

diam["]	Flux	Peak	Image: Flux	Peak	Residual Rms	Fidelity
16	731.256	33.439	733.858	33.158	0.123	270
16	731.256	33.439	733.245	33.167	0.122	272
16	731.256	33.439	733.187	33.160	0.122	272
32	731.596	11.550	783.866	11.515	0.272	42
32	731.596	11.550	739.195	11.432	0.185	62
32	731.596	11.550	750.449	11.484	0.146	79
40	731.620	7.964	793.246	7.641	0.485	16
40	731.620	7.964	681.650	7.617	0.319	24
40	731.620	7.964	756.101	7.809	0.129	61

Table 3: Amplitude fluctuations from pointing errors. Mosaicing with CARMA D-configuration at 230 GHz using single pointing mosaic. For each noise level we list three methods: i) MEM deconvolution with total flux constraint, 732.069 Jy, ii) using single dish as a default image, iii) joint deconvolution of interferometer and single dish data.

Gain[%]	diam[″]	Flux	Peak	Image: Flux	Peak	Residual Rms	Fidelity
1	32	731.596	11.550	784.346	11.508	0.308	37
1	32	731.596	11.550	739.353	11.432	0.197	58
1	32	731.596	11.550	748.258	11.481	0.150	77
5	32	731.597	11.318	788.643	11.213	0.337	33
5	32	731.597	11.318	742.116	11.147	0.228	49
5	32	731.597	11.318	735.909	11.072	0.289	38
10	32	731.599	11.093	817.227	11.044	0.447	25
10	32	731.599	11.093	769.289	11.001	0.318	35
10	32	731.599	11.093	756.887	10.893	0.411	27
20	32	731.596	11.550	918.837	12.208	0.633	19
20	32	731.596	11.550	873.751	12.157	0.531	23
20	32	731.596	11.550	817.280	11.889	0.558	21
1	64	731.652	3.571	780.894	2.792	0.152	18
1	64	731.652	3.571	579.972	2.767	0.134	21
1	64	731.652	3.571	621.134	2.937	0.131	22
5	64	731.652	3.533	781.109	2.800	0.154	18
5	64	731.652	3.533	579.298	2.771	0.138	20
5	64	731.652	3.533	567.089	2.597	0.131	20
10	64	731.653	3.496	784.198	2.849	0.163	17
10	64	731.653	3.496	583.098	2.820	0.147	19
10	64	731.653	3.496	579.028	2.635	0.147	18

Table 4: Mosaicing with CARMA D-configuration at 230 GHz using a 7-pointing mosaic. For each source size and gain fluctuation, we list four methods: i) MEM deconvolution with total flux constraint, 732.069 Jy, ii) using single dish as a default image, iii) joint deconvolution of interferometer and single dish data, iv) combining single dish and mosaic images using *immerge*.

Gain[%]	diam[″]	Flux	Peak	Image: Flux	Peak	Residual Rms	Fidelity
5	32	731.597	11.362	755.302	11.317	0.060	189
5	32	731.597	11.362	749.625	11.299	0.056	202
5	32	731.597	11.362	740.791	11.271	0.052	217
5	32	731.597	11.362	739.663	11.275	0.056	201
1	64	731.652	3.586	813.512	3.412	0.228	15
1	64	731.652	3.586	765.436	3.512	0.091	39
1	64	731.652	3.586	770.717	3.496	0.062	56
1	64	731.652	3.586	755.329	3.399	0.148	23
5	64	731.652	3.548	816.323	3.378	0.227	15
5	64	731.652	3.548	766.323	3.471	0.092	38
5	64	731.652	3.548	785.112	3.359	0.213	16
5	64	731.652	3.548	727.607	3.349	0.142	24
10	64	731.652	3.511	820.173	3.373	0.233	14
10	64	731.652	3.511	771.110	3.457	0.103	34
10	64	731.652	3.511	787.124	3.353	0.224	15
10	64	731.652	3.511	758.052	3.371	0.158	21

Table 5: Mosaicing Simulations for Cas A at 230 GHz. Mosaicing with CARMA 23-antenna DZ configuration using a single pointing mosaic. For each source size we lists four methods: i) MEM deconvolution with total flux constraint, 732.069 Jy, ii) using single dish as a default image, iii) joint deconvolution of interferometer and single dish data. iv) combining single dish and mosaic images using *immerge*.

Gain[%]	diam["]	Flux	Peak	Image: Flux	Peak	Residual Rms	Fidelity
1	64	731.652	3.571	710.066	3.491	0.017	205
1	64	731.652	3.571	758.250	3.520	0.018	196
1	64	731.652	3.571	734.999	3.496	0.017	206
1	64	731.652	3.571	732.773	3.499	0.020	175
5	64	731.652	3.533	709.758	3.452	0.032	108
5	64	731.652	3.533	760.042	3.480	0.034	102
5	64	731.652	3.533	705.745	3.452	0.032	108
5	64	731.652	3.533	721.532	3.463	0.034	102
10	64	731.653	3.496	719.707	3.437	0.057	60
10	64	731.653	3.496	768.895	3.465	0.060	58
10	64	731.653	3.496	717.084	3.439	0.056	61
10	64	731.653	3.496	732.499	3.454	0.057	61

Primary Beam Response for Mosaic Images
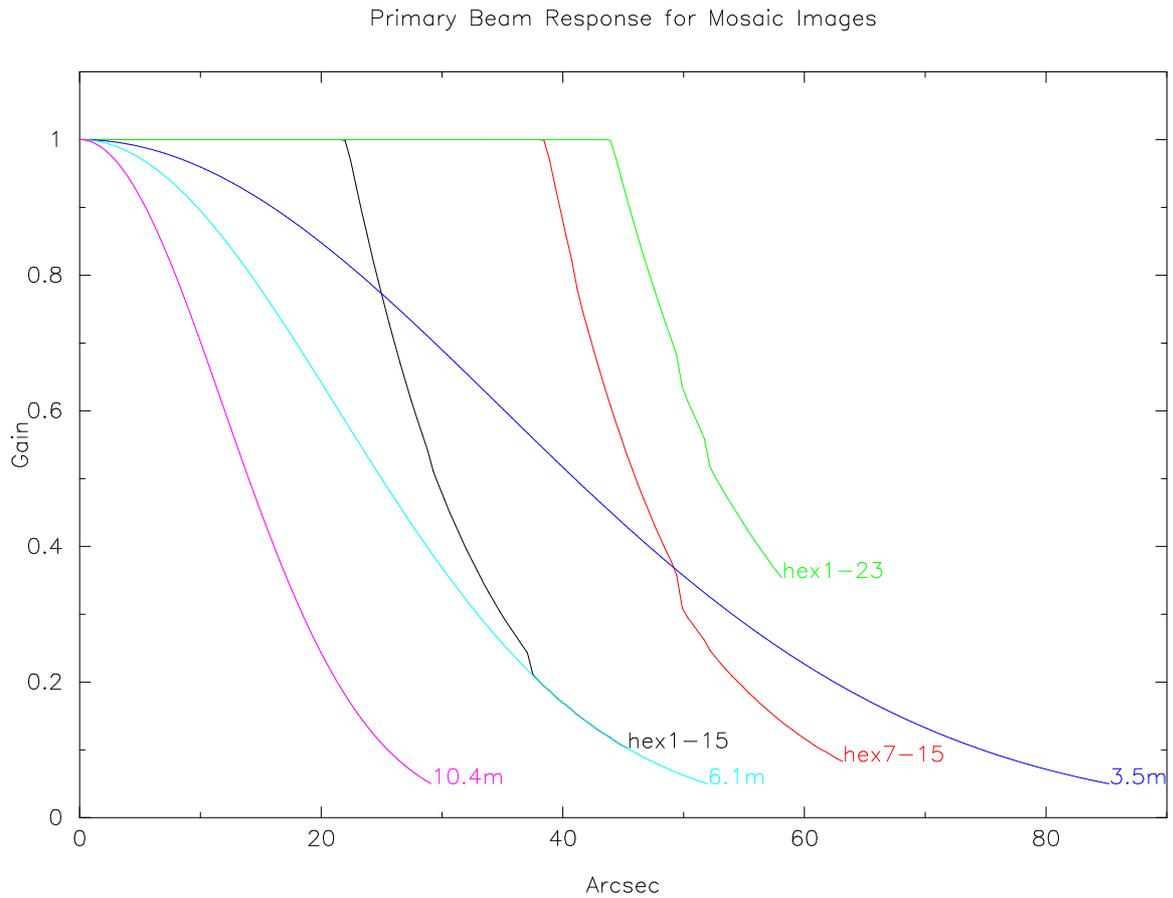
Fig. 1.— Primary beam response for a single pointing mosaic with six 10.4 and nine 6.1m antennas (hex1-15), a 7-pointing hexagonal mosaic with 15 antennas (hex7-15), and the 23-antenna CARMA array (hex1-23). The primary beam pattern for 10.4, 6.1 and 3.5m antennas are also plotted for comparison.
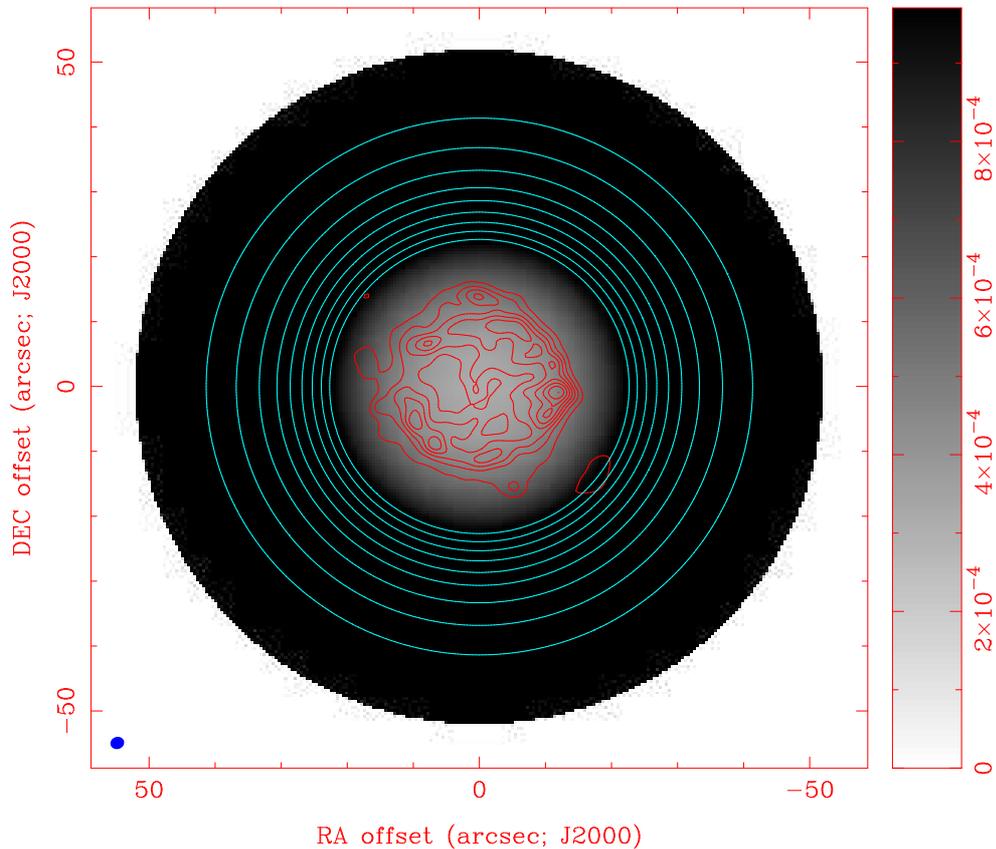
RA, DEC, VELO = 23:23:25.803, 30:00:00.00, 0.00000E+00 km/s at pixel (129.00, 129.00, 1.00)
Spatial region : 1,1 to 257,256
Pixel map image: D.30.casc.vla..041.sen (carma.uv) Min/max=3.226×10^{-4}/9.704×10^{-4} Range = 0 to 9.704×10^{-4} JY/BEAM (
Contour image: D.30.casc.vla..041.cm (carma.uv) Min/max=−0.4422/10.89 JY/BEAM
Contours : 1.362, 2.723, 4.085, 5.446, 6.808, 8.17, 9.531, 10.89
Contour image: D.30.casc.vla..041.gain (carma.uv) Min/max=10^{30}/−10^{30} GAIN
Contours : 0.05, 0.15, 0.25, 0.35, 0.45, 0.55, 0.65, 0.75, 0.85, 0.95

Fig. 2.— Mosaic image of Cas A scaled to 32″ diameter observed with the CARMA 15-antenna D configuration using a single pointing center. Image fidelity, peak/RMS = 27 (see Table 3) Joint deconvolution image with 10% amplitude errors on each antenna (red contours). To avoid noise amplification at the edge of the image MIRIAD does not totally correct for the primary beam to the edge of the mosaic region. The blue contours show the residual primary beam pattern, and the grey scale image shows RMS noise as a function of position. Gaussian beam FWHM in lower left corner.

Fig. 3.— Mosaic image of Cas A scaled to $64''$ diameter observed with the CARMA 15-antenna D configuration using a single pointing center. Joint deconvolution image with 10% amplitude errors on each antenna (red contours). To avoid noise amplification at the edge of the image MIRIAD does not totally correct for the primary beam to the edge of the mosaic region. The blue contours show the residual primary beam pattern, and the grey scale image shows RMS noise as a function of position. Gaussian beam FWHM in lower left corner. A $64''$ diameter source is too large for a single pointing center. Calibration and pointing errors scatter flux out of the source image degrading the image fidelity, peak/RMS = 18 (see Table 3).
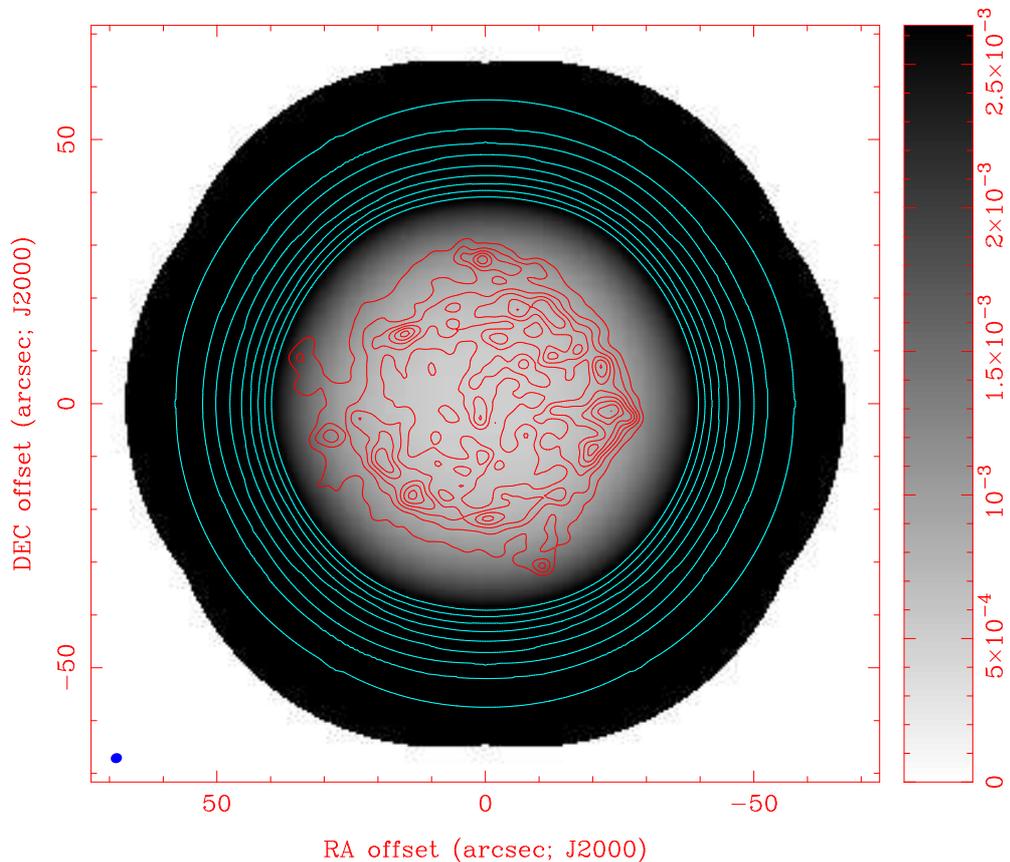
RA, DEC, VELO = 23:23:25.803, 30:00:00.00, 0.00000E+00 km/s at pixel (161.00, 157.00, 1.00)
Spatial region : 1,1 to 321,313
Pixel map image: D.30.casc.vla..08.sen (carma.uv) Min/max=4.897×10⁻⁴/2.636×10⁻³ Range = 0 to 2.636×10⁻³ JY/BEAM (1
Contour image: D.30.casc.vla..08.cm (carma.uv) Min/max=−0.04061/3.496 JY/BEAM
Contours : 0.437, 0.8739, 1.311, 1.748, 2.185, 2.622, 3.059, 3.496
Contour image: D.30.casc.vla..08.gain (carma.uv) Min/max=10³⁰/−10³⁰ GAIN
Contours : 0.05, 0.15, 0.25, 0.35, 0.45, 0.55, 0.65, 0.75, 0.85, 0.95

Fig. 4.— Mosaic image of Cas A scaled to $64''$ diameter observed with the CARMA 15-antenna D configuration using a hex7 pointing pattern. To avoid noise amplification at the edge of the image MIRIAD does not totally correct for the primary beam to the edge of the mosaic region. The blue contours show the residual primary beam pattern, and the grey scale image shows RMS noise as a function of position. Gaussian beam FWHM in lower left corner. With 1% amplitude errors on each antenna a joint deconvolution of interferometer and single dish data gives the best image fidelity. Image fidelity, peak/RMS = 56 (see Table 4).
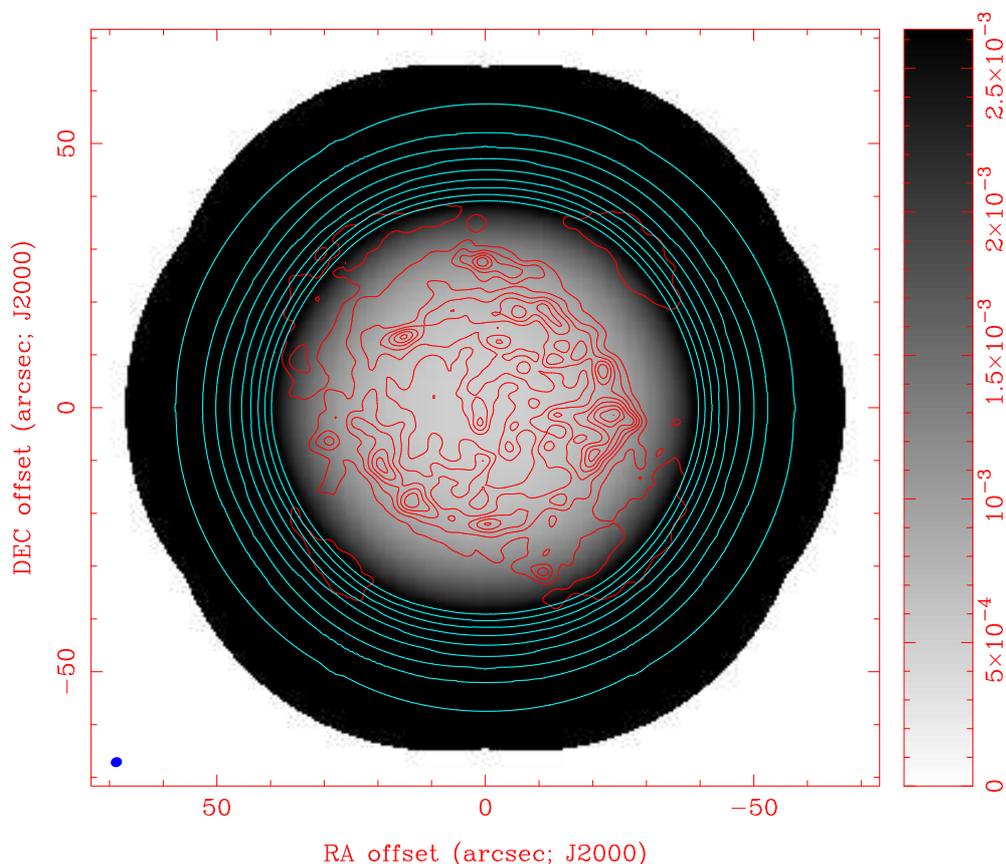
RA, DEC, VELO = 23:23:25.803, 30:00:00.00, 0.00000E+00 km/s at pixel (161.00, 157.00, 1.00)
Spatial region : 1,1 to 321,313
Pixel map image: D.30.casc.vla..081.sen (carma.uv) Min/max=4.897×10⁻⁴/2.636×10⁻³ Range = 0 to 2.636×10⁻³ JY/BEAM (
Contour image: D.30.casc.vla..081.cm (carma.uv) Min/max=−0.1151/3.353 JY/BEAM
Contours : 0.4191, 0.8382, 1.257, 1.676, 2.096, 2.515, 2.934, 3.353
Contour image: D.30.casc.vla..081.gain (carma.uv) Min/max=10³⁰/−10³⁰ GAIN
Contours : 0.05, 0.15, 0.25, 0.35, 0.45, 0.55, 0.65, 0.75, 0.85, 0.95

Fig. 5.— Mosaic image of Cas A scaled to 64″ diameter observed with the CARMA 15-antenna D configuration using a hex7 pointing pattern (red contours). To avoid noise amplification at the edge of the image MIRIAD does not totally correct for the primary beam to the edge of the mosaic region. The blue contours show the residual primary beam pattern, and the grey scale image shows RMS noise as a function of position. Gaussian beam FWHM in lower left corner. With 10% amplitude errors on each antenna the image fidelity is reduced to 15 in a joint deconvolution. Using the single dish data as a default image gives better image fidelity (See table 4).
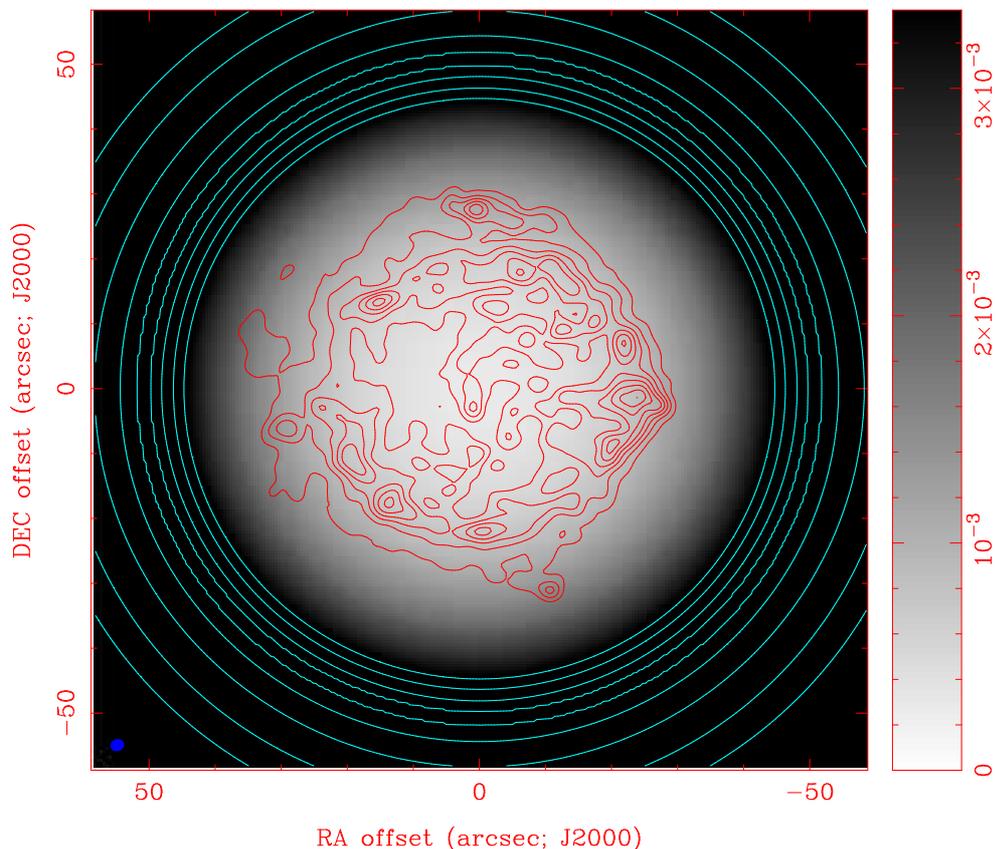
RA, DEC, VELO = 23:23:25.803, 30:00:00.00, 0.00000E+00 km/s at pixel (129.00, 129.00, 1.00)
Spatial region : 1,1 to 257,256
Pixel map image: DZ.30.casc.vla..081.sen (carma.uv) Min/max=$2.915\times10^{-4}/3.345\times10^{-3}$ Range = 0 to 3.345×10^{-3} JY/BEAM
Contour image: DZ.30.casc.vla..081.cm (carma.uv) Min/max=$-0.2284/3.439$ JY/BEAM
Contours : 0.4299, 0.8599, 1.29, 1.72, 2.15, 2.58, 3.009, 3.439
Contour image: DZ.30.casc.vla..081.gain (carma.uv) Min/max=$10^{30}/-10^{30}$ GAIN
Contours : 0.05, 0.15, 0.25, 0.35, 0.45, 0.55, 0.65, 0.75, 0.85, 0.95

Fig. 6.— Mosaic image of Cas A scaled to $64''$ diameter observed with the CARMA 23-antenna DZ configuration using a single pointing center (red contours). To avoid noise amplification at the edge of the image MIRIAD does not totally correct for the primary beam to the edge of the mosaic region. The blue contours show the residual primary beam pattern, and the grey scale image shows RMS noise as a function of position. Gaussian beam FWHM in lower left corner. A joint deconvolution with 10% amplitude errors on each antenna gives and image fidelity 61 (see table 5).
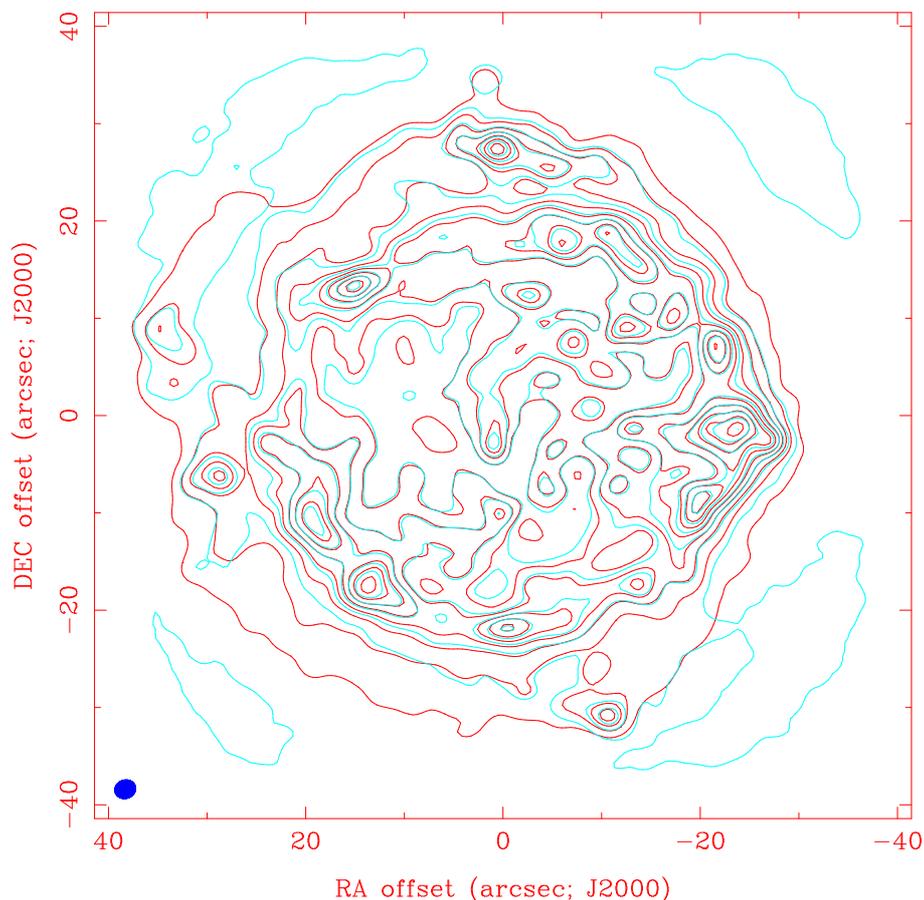
RA, DEC, FREQ = 23:23:25.803, 30:00:00.00, 2.30000000E+02 GHz at pixel (161.00, 157.00, 1.00)
Spatial region : 71,67 to 251,247
Contour image: D.30.casc.vla..0805.regrid (CAS A) Min/max=2.685×10⁻⁵/3.54 JY/BEAM
Contours : 0.177, 0.5309, 0.8849, 1.239, 1.593, 1.947, 2.301, 2.655, 3.009, 3.363
Contour image: D.30.casc.vla..0805.cm (carma.uv) Min/max=10³⁰/−10³⁰ JY/BEAM
Contours : 0.4199, 0.8398, 1.26, 1.68, 2.099, 2.519, 2.939, 3.359

Fig. 7.— Comparison of model (red contours) and mosaic image (blue contours) of Cas A scaled to
64″ diameter observed with the CARMA 15-antenna D configuration using a hex7 pointing pattern.
Gaussian beam FWHM in lower left corner. With 5% amplitude errors on each antenna the image
fidelity is 16 in a joint deconvolution. (See table 4).
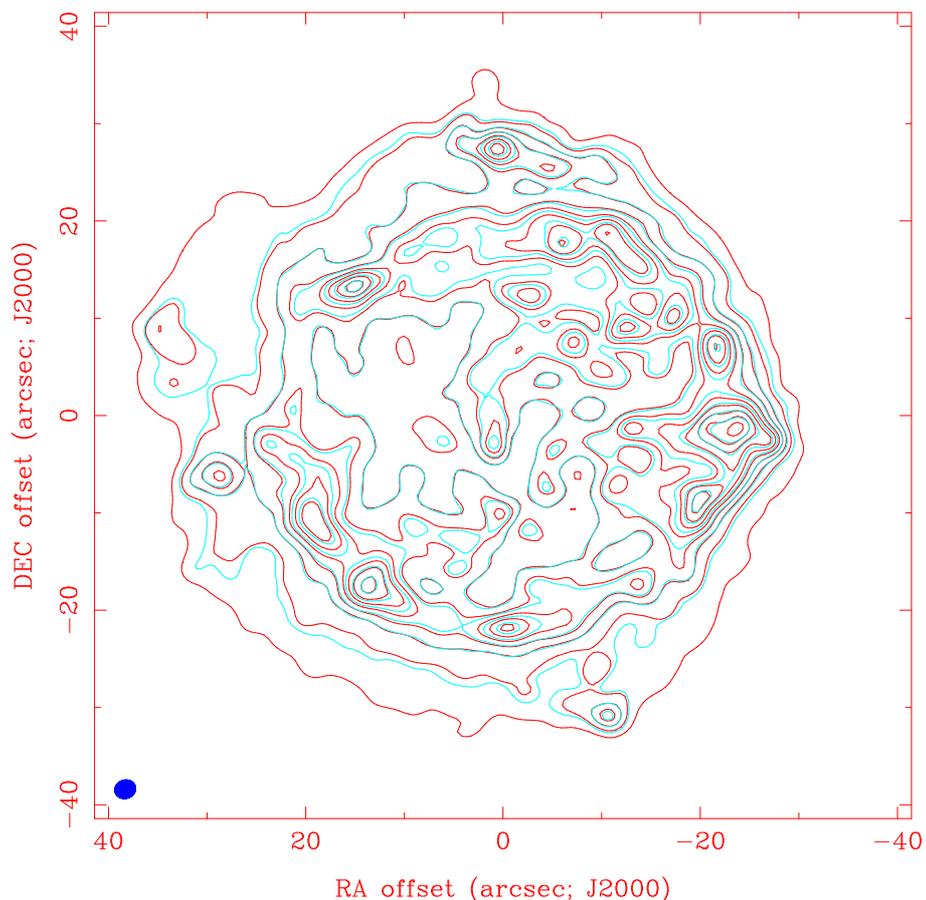
RA, DEC, FREQ = 23:23:25.803, 30:00:00.00, 2.30000000E+02 GHz at pixel (129.00, 129.00, 1.00)
Spatial region : 39,39 to 219,219
Contour image: DZ.30.casc.vla..0805.regrid (CAS A) Min/max=2.66×10^{-5}/3.525 JY/BEAM
Contours : 0.1762, 0.5287, 0.8812, 1.234, 1.586, 1.939, 2.291, 2.644, 2.996, 3.349
Contour image: DZ.30.casc.vla..0805.cm (carma.uv) Min/max=10^{30}/−10^{30} JY/BEAM
Contours : 0.4315, 0.8629, 1.294, 1.726, 2.157, 2.589, 3.02, 3.452

Fig. 8.— Comparison of model (red contours) and mosaic image (blue contours) of Cas A scaled to 64$''$ diameter observed with the CARMA 23-antenna DZ configuration using a single pointing center. Gaussian beam FWHM in lower left corner. With 5% amplitude errors on each antenna the image fidelity is 108 in a joint deconvolution. (See table 5).